Computers & Structures Vol. 33, No. 1, pp. 139–148, 1989
Printed in Great Britain.

0045-7949/89 $3.00 + 0.00

MACRO ELEMENT ANALYSIS OF COMPOSITE BEAM–SLAB SYSTEMS

J. PETROLITO and B. W. GOLLEY
Department of Civil Engineering, University College, Australian Defence Force Academy, Campbell, ACT, Australia

(*Received* 22 *July* 1988)

Abstract—A macro element analysis of fully composite beam–slab systems is presented. The proposed technique combines a macro element which models both the in-plane and transverse behaviour of the slab with a special offset beam element. For the slab macro element, internal displacement functions satisfy the governing equilibrium equations, substantially reducing the number of equations requiring generation and solution. Large elements corresponding to structural units bounded by beams may be used, requiring a minimum of data preparation. The examples considered show that engineering accuracy may be obtained with the generation and solution of very few equations.

INTRODUCTION

Beam–slab construction is in widespread use in both multi-storey buildings and bridges. Typically, the beam is cast monolithically with the slab in the case of all concrete construction, or is connected by shear connectors to the slab in the case of composite steel–concrete construction. In both cases, the beam and slab are generally assumed to act together under any applied loading.

Two types of behaviour occur depending on the relative locations of the beam and slab centrelines.

(1) Full composite action [see Fig. 1(a)]: in this case the beam centreline is eccentric to the slab centreline. When a transverse load is applied to the slab, both horizontal and vertical shear forces are transmitted from the beams to the slab. Hence, in-plane forces in addition to those produced by the bending action are introduced into the slab.

(2) Partial composite action [see Fig. 1(b)]: this is a special case of full composite action and occurs when the centrelines of the beam and slab are coincident. Only vertical shear forces are transmitted from the beams to the slab when a transverse load is applied to the slab. Therefore, only the bending behaviour of the slab needs to be considered as no in-plane forces occur along the neutral axis of the slab.

The governing equations of a beam–slab system were derived by Wood [1]. Although he derived the equations for the full composite action case, the study was primarily concerned with partial composite action. In a series of papers, Allen and Severn [2] derived approximate series solutions for a number of beam–slab configurations. The solutions, however, were for symmetrical loads and restricted boundary conditions. Kretsis [3] used a similar approach to derive some design rules for full composite action. It was clear, however, that any practical problem would require numerical calculations.

Khan and Kemp [4] used the finite difference method to analyse a single square panel beam–slab system with full composite action. Despite the restricted geometry considered, they obtained some useful design guidelines. More recent studies have concentrated on the use of finite elements or finite strips in order to treat more general geometries, e.g. [5–10].

The finite element method appears to be well established in the analysis of bridges, e.g. [11, 12]. However, it appears rare to analyse complete buildings consisting of beams, slabs and columns using finite elements. It is common practice to analyse such buildings as equivalent frames with the slabs contributing some approximately determined stiffness to the beams. The equivalent structure is then analysed using standard beam and column elements. Fraser [13, 14] proposed new formulas for determining the equivalent beam stiffness based on extensive modelling using finite elements.

Hrabok and Hrudley [9] suggest that engineers have been relucant to use the finite element method for the following reasons:

(1) A large number of elements are available, making it difficult to choose the 'best' element.

(2) Engineers lack familiarity and experience with the finite element method.

(3) There is a lack of suitable programs.

To overcome some of the difficulties, Hrabok [8] investigated a large number of plate bending elements and prepared a computer program using twelve degree of freedom hybrid stress elements, which he considered most suitable for analysing floor systems. However, a large number of elements is still required in the analysis.

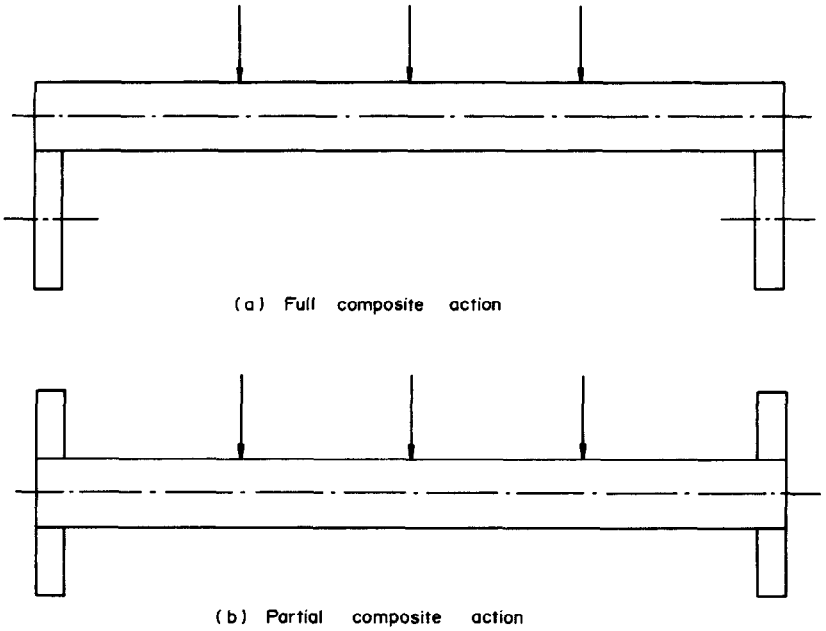

Fig. 1. Behaviour of beam–slab systems.

The number of elements required can be reduced by using macro elements. In previous papers [15, 16], the authors have presented macro elements which may be used to analyse plate bending and two-dimensional stress problems. These elements are combined in this paper with a special beam element derived below to allow for the efficient analysis of fully composite beam–slab systems.

ANALYSIS ASSUMPTIONS

Figure 2 shows a typical beam–slab junction. Node 1 is the reference node for the two elements and lies on the centreline of the plate. The centreline of the beam is offset vertically by a distance f from the plate centreline. Node 1′ is in line with node 1 and is on the vertical centreline of the beam.

In deriving the beam properties, the following assumptions are made:

(1) the beam and slab are rigidly connected;

(2) the width of the beam, c, is small so that nodes 1 and 1′ can be taken as coincident;

(3) no distortion of the beam cross-section occurs as the structure deforms;

(4) major axis bending effects dominate and minor axis bending can be neglected;

(5) the torsion behaviour is governed by St. Venant's torsion theory;

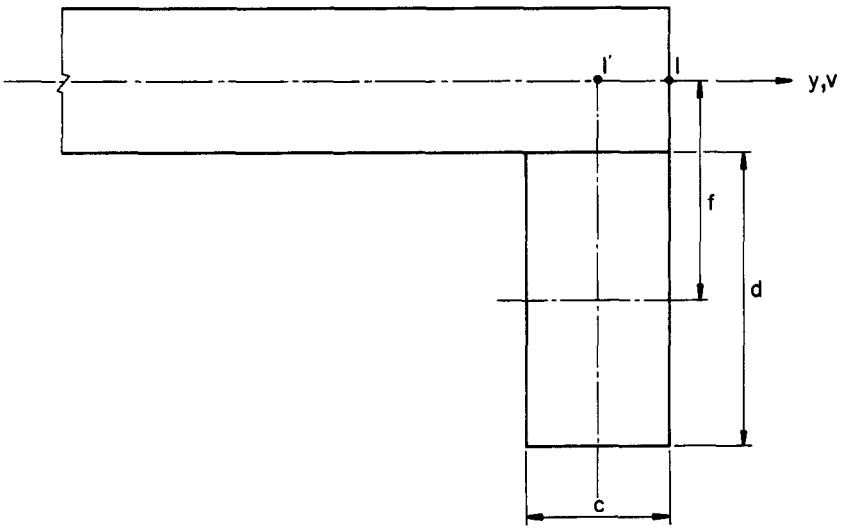

Fig. 2. Beam–slab junction.

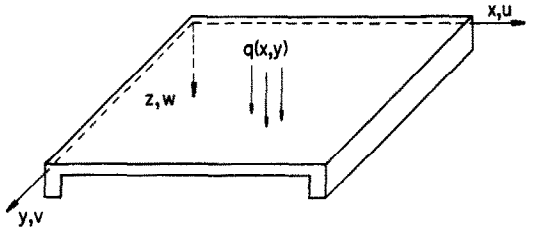

Fig. 3. Sign convention.

(6) no coupling occurs between the bending and torsion modes.

While the above assumptions are not valid for a general configuration, they are realistic for practical geometries [1, 4]. As a consequence of assumption (4), no strain energy is associated with the displacement v, which is perpendicular to the minor axis of the beam. Hence, this displacement component need not be considered when deriving the beam properties.

GOVERNING EQUATIONS

Figure 3 shows the sign convention used for the governing equations of the beam–slab system.

Plate bending theory

The transverse bending behaviour of the slab is assumed to be governed by thin plate theory [17]. The transverse deflection, $w(x, y)$, of a plate lying in the xy plane is governed by the equation

$$w_{,xxxx} + 2w_{,xxyy} + w_{,yyyy} = \frac{q}{D}, \tag{1}$$

where $q(x, y)$ is the applied transverse load and D is the plate rigidity.

Plane stress theory

The in-plane behaviour of the slab is assumed to be governed by plane stress theory [18]. Assuming zero in-plane body forces, the equilibrium equations for a plate lying in the xy plane, expressed in terms of in-plane displacements $u(x, y)$ and $v(x, y)$, are

$$u_{,xx} + \frac{(1-\nu)}{2}u_{,yy} + \frac{(1+\nu)}{2}v_{,xy} = 0$$

$$v_{,yy} + \frac{(1-\nu)}{2}v_{,xx} + \frac{(1+\nu)}{2}u_{,xy} = 0, \tag{2}$$

where ν is Poisson's ratio.

Beam theory

For beam bending, plane sections are assumed to remain plane and the cross-section is assumed to remain distortion free. Beam torsion is assumed to be governed by St. Venant's torsion.

SLAB ELEMENT FORMULATION

The approximations for the slab element are detailed below. Only an outline of the slab element formulation is given below; full details were given previously [15, 16]. Figure 4 shows a typical slab element, e, and the degrees of freedom associated with the polynomial shape functions for both transverse and in-plane behaviour. In the following a subscript b refers to a plate bending approximation while a subscript i refers to an in-plane approximation.

Plate bending approximation

The transverse displacement approximation is made up of four solutions, namely:

(1) A polynomial solution which satisfies the homogeneous form of eqn (1) and approximates the displacement as a cubic polynomial. The shape functions of the ACM element [12] are used with nodal variables

$$\boldsymbol{\phi}^e_{pb} = \{w^e_1, \theta^e_{x1}, \theta^e_{y1}, w^e_2, \theta^e_{x2}, \theta^e_{y2}, w^e_3, \theta^e_{x3}, \theta^e_{y3}, w^e_4, \theta^e_{x4}, \theta^e_{y4}\} \tag{3}$$

which are common to adjacent elements (see Fig. 4).

(2) A trigonometric series solution associated with constrained sinusoidal displacements on the sides of the element which satisfies the homogeneous form of eqn (1). This solution is chosen to produce zero rotations at the corners of the element. For the mth term in the series, the shape functions are expressed in terms of generalized side displacement variables

$$\boldsymbol{\phi}^e_{btm} = \{\phi^e_{btm12}, \phi^e_{btm23}, \phi^e_{btm34}, \phi^e_{btm14}\} \tag{4}$$

which are common to adjacent elements. The subscripts 12, 23, etc. refer to sides between corner nodes 1 and 2, 2 and 3 etc. A total of M_w terms of the series is used.

(3) A trigonometric series solution associated with sinusoidal normal moments and zero displacements on the side of the element which satisfies the homogeneous form of eqn (1). For the mth term in the series, the shape functions are expressed in terms of generalized side moment variables

$$\boldsymbol{\phi}^e_{bnm} = \{\phi^e_{bnm12}, \phi^e_{bnm23}, \phi^e_{bnm34}, \phi^e_{bnm14}\}. \tag{5}$$

These variables are local to each element. A total of M_m terms of the series is used.

(4) A particular solution, $w^e_0(x, y)$ associated with the transverse load on the slab. This is taken as either a Levy series solution or a Navier series solution as appropriate [17]. Combining the above solutions, the transverse displacement is approximated by

$$w^e = \mathbf{N}^e_{bp}(x, y)\boldsymbol{\phi}^e_{bp} + \sum_{m=1}^{M_w} \mathbf{N}^e_{btm}(x, y)\boldsymbol{\phi}^e_{btm} + \sum_{m=1}^{M_m} \mathbf{N}^e_{bnm}(x, y)\boldsymbol{\phi}^e_{bnm} + w^e_0(x, y). \tag{6}$$

The above approximation is complete, i.e. as M_w and M_m approach infinity any specified displacement function within a rectangular region may be represented.

The approximation taken in eqn (6) ensures that transverse displacements are C_1 continuous at the corners of the element, but only C_0 continuous on the sides of the element. To enforce C_1 continuity on the sides, weighted integrals of the side normal rotations are introduced which are made common to adjacent elements [15]. A total of M_m of these weighted integrals is introduced on each side of the element. Eliminating the series moment variables at the local level enables the stiffness matrix and load vector associated with slab bending to be calculated using the total potential energy principle.

The final element variables are the polynomial variables, ϕ_{bp}, the series transverse displacement variables, ϕ_{btm}, and the new weighted integral variables denoted by θ_{bnm}. The stiffness equations for the bending approximation for the element can be expressed as

$$\begin{Bmatrix} \mathbf{R}^e_{bp} \\ \mathbf{R}^e_{bt} \\ \mathbf{R}^e_{bn} \end{Bmatrix} = \begin{bmatrix} \mathbf{K}^e_{bpp} & \mathbf{K}^e_{bpt} & \mathbf{K}^e_{bpn} \\ & \mathbf{K}^e_{btt} & \mathbf{K}^e_{btn} \\ \text{Symm.} & & \mathbf{K}^e_{bnn} \end{bmatrix} \begin{Bmatrix} \boldsymbol{\phi}^e_{bp} \\ \boldsymbol{\phi}^e_{bt} \\ \boldsymbol{\theta}^e_{bn} \end{Bmatrix} \tag{7}$$

or

$$\mathbf{R}^e_b = \mathbf{K}^e_b \boldsymbol{\phi}^e_b, \tag{8}$$

where $\boldsymbol{\phi}^e_{bt} = \{\boldsymbol{\phi}^e_{bt1}, \boldsymbol{\phi}^e_{bt2}, \ldots, \boldsymbol{\phi}^e_{btM_u}\}$ and $\boldsymbol{\theta}^e_{bn} = \{\boldsymbol{\theta}^e_{bn1}, \boldsymbol{\theta}^e_{bn2}, \ldots, \boldsymbol{\theta}^e_{bnM_m}\}$. $\mathbf{R}^e_b$ and $\mathbf{K}^e_b$ are the load vector and stiffness matrix for the slab associated with transverse bending effects.

In-plane approximation

The in-plane approximation is made up of three solutions, namely:

(1) A polynomial solution which satisfies the homogeneous form of eqn (2). The tangential displacement on each side of the element is taken as a quadratic polynomial in terms of the nodal variables

$$\boldsymbol{\phi}^e_{pb} = \{u^e_1, v^e_1, u^e_2, u^e_3, v^e_3, v^e_4, u^e_5, v^e_5, u^e_6, u^e_7, v^e_7, v^e_8\} \tag{9}$$

which are common to adjacent elements (see Fig. 4).

(2) A trigonometric series solution associated with constrained cosinusoidal tangential displacements on the sides of the element which satisfies the homogeneous form of eqn (2). This solution is chosen to produce zero displacements at the corners of the element. For the mth term in the series, the shape functions are expressed in terms of generalized side tangential displacement variables

$$\boldsymbol{\phi}^e_{itm} = \{\phi^e_{itm12}, \phi^e_{itm23}, \phi^e_{itm34}, \phi^e_{itm14}\} \tag{10}$$

which are common to adjacent elements. A total of M_u terms of the series is used.

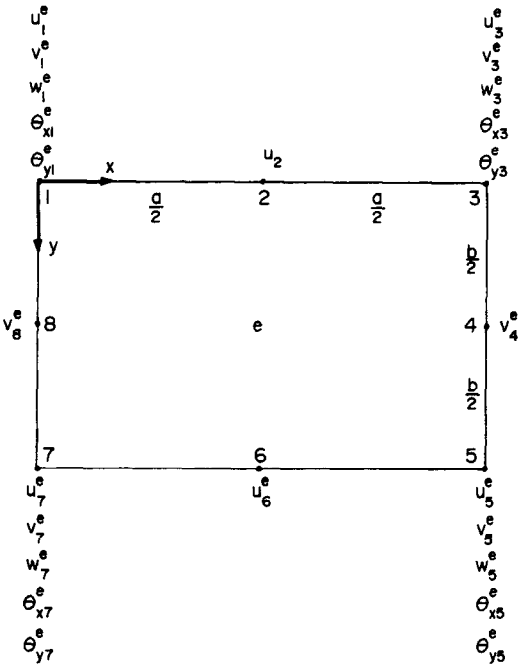

Fig. 4. Typical slab element and polynomial degrees of freedom.

(3) A trigonometric series solution associated with sinusoidal normal stresses and zero tangential displacements on the sides of the element which satisfies the homogeneous form of eqn (2). For the mth term in the series, the shape functions are expressed in terms of generalized side stress variables

$$\boldsymbol{\phi}^e_{inm} = \{\phi^e_{inm12}, \phi^e_{inm23}, \phi^e_{inm34}, \phi^e_{inm14}\}. \tag{11}$$

These variables are local to each element. A total of M_s terms of the series is used. Combining the above solutions, the in-plane displacements are approximated by

$$u^e = \mathbf{N}^e_{ip}(x,y)\boldsymbol{\phi}^e_{ip} + \sum_{m=1}^{M_u} \mathbf{N}^e_{itm}(x,y)\boldsymbol{\phi}^e_{itm} + \sum_{m=1}^{M_s} \mathbf{N}^e_{inm}(x,y)\boldsymbol{\phi}^e_{inm}$$

$$v^e = \bar{\mathbf{N}}^e_{ip}(x,y)\boldsymbol{\phi}^e_{ip} + \sum_{m=1}^{M_u} \bar{\mathbf{N}}^e_{itm}(x,y)\boldsymbol{\phi}^e_{itm} + \sum_{m=1}^{M_s} \bar{\mathbf{N}}^e_{inm}(x,y)\boldsymbol{\phi}^e_{inm}. \tag{12}$$

As with the bending approximation, the above approximation is complete.

The approximation taken in eqn (12) ensures that in-plane displacements are continuous at the corners of the element, but only tangential displacements are continuous on the sides of the element. To enforce continuity of normal displacements on the sides, weighted integrals of the side normal displacements

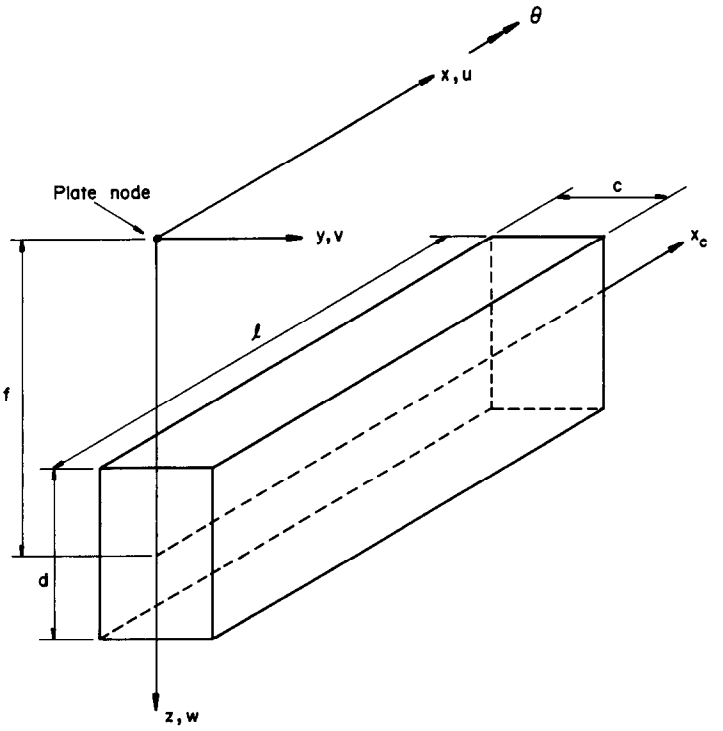

Fig. 5. Axis system for beam element.

are introduced which are made common to adjacent elements [16]. A total of M_s of these weighted integrals is introduced on each side of the element. Eliminating the series stress variables at the local level enables the stiffness matrix and load vector associated with the in-plane behaviour of the slab to be calculated using the total potential energy principle.

The final element variables for in-plane effects are the polynomial variables, ϕ_{ip}, the series tangential displacement variables, ϕ_{itm}, and the new weighted integral variables denoted by $\bar{\phi}_{in}$. The stiffness equations for the in-plane approximation of the element can be expressed as

$$\begin{Bmatrix} \mathbf{R}^e_{ip} \\ \mathbf{R}^e_{it} \\ \mathbf{R}^e_{in} \end{Bmatrix} = \begin{bmatrix} \mathbf{K}^e_{ipp} & \mathbf{K}^e_{ipt} & \mathbf{K}^e_{ipn} \\ & \mathbf{K}^e_{itt} & \mathbf{K}^e_{itn} \\ \text{Symm.} & & \mathbf{K}^e_{inn} \end{bmatrix} \begin{Bmatrix} \boldsymbol{\phi}^e_{ip} \\ \boldsymbol{\phi}^e_{it} \\ \bar{\boldsymbol{\phi}}^e_{in} \end{Bmatrix} \tag{13}$$

or

$$\mathbf{R}^e_i = \mathbf{K}^e_i \boldsymbol{\phi}^e_i \tag{14}$$

where $\boldsymbol{\phi}^e_{it} = \{\phi^e_{it1}, \phi^e_{it2}, \ldots, \phi^e_{itM_u}\}$ and $\bar{\boldsymbol{\phi}}^e_{in} = \{\bar{\phi}^e_{in1}, \bar{\phi}^e_{in2}, \ldots, \bar{\phi}^e_{inM_s}\}$. $\mathbf{R}^e_i$ and $\mathbf{K}^e_i$ are the load vector and stiffness matrix for the slab associated with in-plane effects.

BEAM ELEMENT FORMULATION

Figure 5 shows the axis system for a typical beam element. The x axis, which coincides with the middle surface of the adjoining slab, is offset vertically by a distance f from the beam's centroidal axis, x_c. The length of the beam, l, equals a or b depending on the length of the adjoining slab element. The beam element uses combinations of polynomial and trigonometric shape functions with the final element degrees of freedom being displacement parameters only.

In contrast to the slab element, the assumed displacement functions for the beam element do not satisfy the appropriate governing differential equations. The loads on the beam consist of two components, namely the loads directly applied to the beam plus the loads applied by the adjoining slab. Since the interaction loads are initially unknown, it is impossible to satisfy the governing differential equations for the beam.

Figure 6 shows the geometry and nodal variables associated with the polynomial terms for the beam element. For simplicity, only transverse loads (i.e. loads acting in the z direction) are assumed to be applied to the beam as these are the only ones likely to arise in practice. However, other loads are readily incorporated in a similar manner.

The beam stiffness matrix is derived by making independent assumptions regarding the displacements u^e and w^e and the rotation θ^e about its longitudinal axis, x.

Firstly, the axial displacement, u^e, is approximated by the sum of quadratic polynomials plus a truncated cosine series which is constrained such that displacements are zero at the ends of the element. Thus u^e is

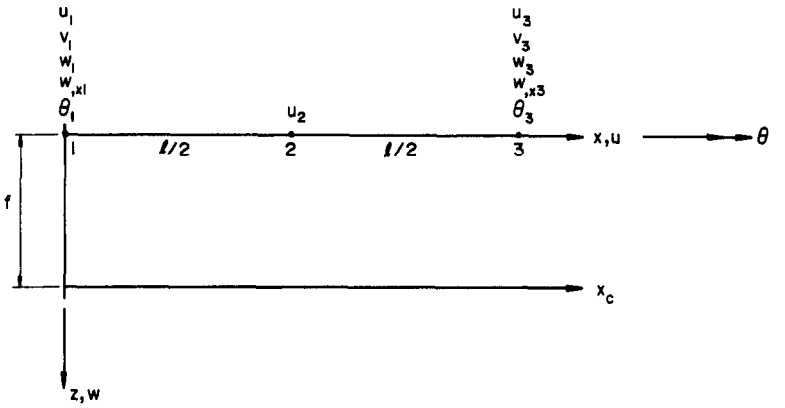

Fig. 6. Typical beam element and polynomial degrees of freedom.

approximated by

$$u^e = \mathbf{N}^e_{pu}(x)\boldsymbol{\phi}^e_{pu} + \sum_{m=1}^{M_u} \phi^e_{um} \times\left[\cos\left(\frac{m\pi x}{l}\right) - \frac{(2x-l)(x-l)+(-1)^m x(2x-l)}{l^2}\right]. \tag{15}$$

The terms in $\mathbf{N}^e_{pu}$ are quadratic Lagrangian shape functions [12] and $\boldsymbol{\phi}^e_{pu} = \{u^e_1, u^e_2, u^e_3\}$. The approximation given in eqn (15) ensures that the axial displacement of the beam is compatible with the tangential displacement of the adjacent slab element, providing the number of terms in the constrained cosine series, M_u, is the same for the beam and slab.

Secondly, the transverse displacement, w^e, is approximated by the sum of cubic polynomials plus a truncated sine series which is constrained such that the rotation, $w_{,x}$, is zero at the ends of the element. Thus w^e is approximated by

$$w^e = \mathbf{N}^e_{pw}(x)\boldsymbol{\phi}^e_{pw} + \sum_{m=1}^{M_w} \phi^e_{wm} \times\left[\sin\left(\frac{m\pi x}{l}\right) - \frac{m\pi(x(l-x)^2-(-1)^m x^2(l-x))}{l^3}\right]. \tag{16}$$

The terms in $\mathbf{N}^e_{pw}$ are the cubic Hermite shape functions for beam bending [12] and $\boldsymbol{\phi}^e_{pw} = \{w^e_1, w^e_{,x1}, w^e_3, w^e_{,x3}\}$.

The approximation given in eqn (16) ensures that the transverse displacement of the beam is compatible with the transverse displacement of the adjacent slab element, providing the number of terms in the constrained sine series, M_w, is the same for the beam and slab. It also ensures that normal rotations about the y axis are compatible at the corners of the beam and slab.

Finally, the rotation of the beam about the x axis, θ^e, is approximated by a linear function plus a truncated sine series. Thus θ^e is approximated by

$$\theta^e = \theta^e_1\left(1-\frac{x}{l}\right) + \theta^e_3\left(\frac{x}{l}\right) + \sum_{m=1}^{M_\theta} \frac{2}{l}\phi^e_{\theta m}\sin\left(\frac{m\pi x}{l}\right) \tag{17}$$

where a factor of $2/l$ has been introduced for convenience as discussed later. Equating the variables θ^e_1 and θ^e_3 to the corner rotations of the adjacent slab element ensures that transverse displacements are C_1 continuous at corners. As discussed previously, the continuity of normal rotations for the slab elements is only achieved in a weighted integral sense. Similarly, when beams are present, the continuity of the normal slab rotation and the beam rotation on the sides of the elements is only achieved in a weighted integral sense.

From eqns (15), (16) and (17), the beam approximations can be written in a compact form as

$$\begin{aligned} u^e &= \mathbf{N}^e_u(x)\boldsymbol{\phi}^e_u \\ w^e &= \mathbf{N}^e_w(x)\boldsymbol{\phi}^e_w \\ \theta^e &= \mathbf{N}^e_\theta(x)\boldsymbol{\phi}^e_\theta, \end{aligned} \tag{18}$$

where

$$\begin{aligned} \boldsymbol{\phi}^e_u &= \{u^e_1, u^e_2, u^e_3, \phi^e_{u1}, \phi^e_{u2}, \ldots, \phi^e_{uM_u}\} \\ \boldsymbol{\phi}^e_w &= \{w^e_1, w^e_{,x1}, w^e_3, w^e_{,x3}, \phi^e_{w1}, \phi^e_{w2}, \ldots, \phi^e_{wM_w}\} \\ \boldsymbol{\phi}^e_\theta &= \{\theta^e_1, \theta^e_3, \phi^e_{\theta 1}, \phi^e_{\theta 2}, \ldots, \phi^e_{\theta M_\theta}\}. \end{aligned} \tag{19}$$

The element displacement approximations are defined relative to the x axis as shown in Fig. 5. To establish the beam properties, it is convenient to refer all displacements to the centroidal axis of the beam, x_c. If the cross-section of the beam is assumed to be rigid, the two sets of displacements are related by the

following transformation rules:

$$u_c^e = u^e - f^e \frac{dw^e}{dx}$$

$$w_c^e = w^e$$

$$\theta_c^e = \theta^e, \tag{20}$$

where u_c^e, w_c^e and θ_c^e are the displacements and rotation relative to the centroidal axis, x_c. Substituting eqn (18) into eqn (20) gives

$$u_c^e = \mathbf{N}_u^e(x)\boldsymbol{\phi}_u^e - f^e \frac{d\mathbf{N}_w^e(x)}{dx}\boldsymbol{\phi}_w^e$$

$$w_c^e = \mathbf{N}_w^e(x)\boldsymbol{\phi}_w^e$$

$$\theta_c^e = \mathbf{N}_\theta^e(x)\boldsymbol{\phi}_\theta^e. \tag{21}$$

The total potential energy of the beam, Π^e, is

$$\Pi^e = \frac{1}{2}\int_0^l \left[A^e E^e \left(\frac{du_c^e}{dx}\right)^2 + E^e I_{yy}^e \left(\frac{d^2 w_c^e}{dx^2}\right)^2 + G^e J^e \left(\frac{d\theta_c^e}{dx}\right)^2\right] dx - \int_0^l p_w^e w^e \, dx, \tag{22}$$

where p_w^e is the applied transverse load on the beam. Substituting eqn (21) into eqn (22) and performing the integration gives

$$\Pi^e = \tfrac{1}{2}\{\boldsymbol{\phi}_u^e \boldsymbol{\phi}_w^e \boldsymbol{\phi}_\theta^e\}^T \begin{bmatrix} \mathbf{K}_{uu}^e & \mathbf{K}_{uw}^e & \mathbf{0} \\ \mathbf{K}_{uw}^{eT} & \mathbf{K}_{ww}^e & \mathbf{0} \\ \mathbf{0} & \mathbf{0} & \mathbf{K}_{\theta\theta}^e \end{bmatrix} \times \begin{Bmatrix} \boldsymbol{\phi}_u^e \\ \boldsymbol{\phi}_w^e \\ \boldsymbol{\phi}_\theta^e \end{Bmatrix} - \{\boldsymbol{\phi}_u^e \boldsymbol{\phi}_w^e \boldsymbol{\phi}_\theta^e\}^T \begin{Bmatrix} \mathbf{0} \\ \mathbf{R}_w^e \\ \mathbf{0} \end{Bmatrix} \tag{23}$$

or

$$\Pi^e = \tfrac{1}{2}\boldsymbol{\phi}^{eT}\mathbf{K}^e\boldsymbol{\phi}^e - \boldsymbol{\phi}^{eT}\mathbf{R}^e, \tag{24}$$

where $\boldsymbol{\phi}^e = \{\boldsymbol{\phi}_u^e, \boldsymbol{\phi}_w^e, \boldsymbol{\phi}_\theta^e\}$ and $\mathbf{K}^e$ is a symmetrical matrix. The submatrices in eqn (23) are given by

$$\mathbf{K}_{uu}^e = \int_0^l A^e E^e \frac{d\mathbf{N}_u^{eT}}{dx}\frac{d\mathbf{N}_u^e}{dx} dx$$

$$\mathbf{K}_{uw}^e = -\int_0^l f^e A^e E^e \frac{d\mathbf{N}_u^{eT}}{dx}\frac{d^2\mathbf{N}_w^e}{dx^2} dx$$

$$\mathbf{K}_{ww}^e = \int_0^l [(f^e)^2 A^e E^e + E^e I_{yy}^e]\frac{d^2\mathbf{N}_w^{eT}}{dx^2}\frac{d^2\mathbf{N}_w^e}{dx^2} dx$$

$$\mathbf{K}_{\theta\theta}^e = \int_0^l G^e J^e \frac{d\mathbf{N}_\theta^{eT}}{dx}\frac{d\mathbf{N}_\theta^e}{dx} dx$$

$$\mathbf{R}_w^e = \int_0^l p_w^e \mathbf{N}_w^{eT} dx. \tag{25}$$

As can be seen from eqn (23), the axial and transverse effects are coupled in the general case when the beam centreline is offset from the slab centreline. In the simpler case when both centrelines coincide ($f^e = 0$), the bending and in-plane modes uncouple and they can be analysed separately.

The contribution to Π^e associated with $\boldsymbol{\phi}_\theta^e$ can be written in partitioned form as

$$\Pi_\theta^e = \tfrac{1}{2}\{\boldsymbol{\phi}_i^e \boldsymbol{\phi}_j^e\}^T \begin{bmatrix} \mathbf{K}_{ii}^e & \mathbf{K}_{ij}^e \\ \mathbf{K}_{ij}^{eT} & \mathbf{K}_{jj}^e \end{bmatrix} \begin{Bmatrix} \boldsymbol{\phi}_i^e \\ \boldsymbol{\phi}_j^e \end{Bmatrix}, \tag{26}$$

where $\boldsymbol{\phi}_i^e = \{\theta_1^e, \theta_3^e\}$ and $\boldsymbol{\phi}_j^e = \{\phi_{01}^e, \phi_{02}^e, \ldots, \phi_{0M_m}^e\}$. To enforce continuity of normal rotations on the beam and the adjacent plate element, weighted integrals of the rotation of the beam about the x axis are introduced. In accordance with the definition used in [15], weighted integrals of rotation, $\boldsymbol{\phi}_n^e$, are defined as

$$\boldsymbol{\phi}_n^e = \int_0^l \boldsymbol{\lambda}^e\left(\frac{x}{l}\right)\left[\theta^e - \theta_1^e\left(1 - \frac{x}{l}\right) - \theta_2^e\left(\frac{x}{l}\right)\right] dx, \tag{27}$$

where

$$\boldsymbol{\lambda}\left(\frac{x}{l}\right) = \left\{\sin\left(\frac{\pi x}{l}\right), \sin\left(\frac{2\pi x}{l}\right), \ldots, \sin\left(\frac{(M_m - 2)\pi x}{l}\right), \left(1 - \frac{x}{l}\right), \left(\frac{x}{l}\right)\right\}, \quad M_m > 2$$

$$\boldsymbol{\lambda}\left(\frac{x}{l}\right) = \left\{\left(1 - \frac{x}{l}\right), \left(\frac{x}{l}\right)\right\}, \quad M_m = 2$$

$$\boldsymbol{\lambda}\left(\frac{x}{l}\right) = \left\{\sin\left(\frac{\pi x}{l}\right)\right\}, \quad M_m = 1. \tag{28}$$

In eqn (27), a linear function of the two end rotations, θ_1^e and θ_2^e, which are common to the beam and the adjacent slab element, has been subtracted from the total rotation.

Substituting for θ^e from eqn (17) into eqn (27) and performing the integration gives

$$\boldsymbol{\phi}_n^e = \mathbf{W}_j^e \boldsymbol{\phi}_j^e. \tag{29}$$

The weighted integrals of rotation, $\boldsymbol{\phi}_n^e$, are made common to the beam and the adjacent slab element. If $M_m > 2$, $\mathbf{W}_j^e$ contains an identity matrix of size $(M_m - 2) \times (M_m - 2)$ as a submatrix. This is a consequence of the factor of $2/l$ used in eqn (17). This simplifies the subsequent inversion of $\mathbf{W}_j^e$. In addition, the weighted integrals of rotation do not depend on $\boldsymbol{\phi}_i^e$, which is a consequence of the definition used in eqn (27). This reduces the amount of numerical matrix algebra required.

As the variables $\boldsymbol{\phi}_j^e$ are local to the beam, eqn (29) can be solved for $\boldsymbol{\phi}_j^e$ to give

$$\boldsymbol{\phi}_j^e = (\mathbf{W}_j^e)^{-1}\boldsymbol{\phi}_n^e. \tag{30}$$

Substituting for ϕ_j^e from eqn (30) into eqn (26) gives

$$\Pi_\theta^e = \tfrac{1}{2}\{\phi_i^e \phi_n^e\}^T \begin{bmatrix} \mathbf{K}_{ii}^e & \mathbf{K}_{ij}^e \\ \mathbf{K}_{ij}^{eT} & \mathbf{K}_{jj}^e \end{bmatrix} \begin{Bmatrix} \phi_i^e \\ \phi_n^e \end{Bmatrix} \tag{31}$$

or

$$\Pi_\theta^e = \tfrac{1}{2}\bar{\phi}_\theta^{eT} \bar{\mathbf{K}}_{\theta\theta}^e \bar{\phi}_\theta^e, \tag{32}$$

where

$$\bar{\mathbf{K}}_{ij}^e = \mathbf{K}_{ij}^e (\mathbf{W}_j^e)^{-1}$$
$$\bar{\mathbf{K}}_{jj}^e = (\mathbf{W}_j^e)^{-T} \mathbf{K}_{jj}^e (\mathbf{W}_j^e)^{-1} \tag{33}$$

and $\bar{\phi}_\theta^e = \{\phi_i^e, \phi_n^e\}$. The matrix $\bar{\mathbf{K}}_{\theta\theta}^e$ is symmetrical.

Hence the total potential energy of the beam is

$$\Pi^e = \tfrac{1}{2}\{\phi_u^e \phi_w^e \bar{\phi}_\theta^e\}^T \times \begin{bmatrix} \mathbf{K}_{uu}^e & \mathbf{K}_{uw}^e & \mathbf{0} \\ \mathbf{K}_{uw}^{eT} & \mathbf{K}_{ww}^e & \mathbf{0} \\ \mathbf{0} & \mathbf{0} & \bar{\mathbf{K}}_{\theta\theta}^e \end{bmatrix} \begin{Bmatrix} \phi_u^e \\ \phi_w^e \\ \bar{\phi}_\theta^e \end{Bmatrix} - \{\phi_u^e \phi_w^e \bar{\phi}_\theta^e\}^T \begin{Bmatrix} \mathbf{0} \\ \mathbf{R}_w^e \\ \mathbf{0} \end{Bmatrix} \tag{34}$$

or

$$\Pi^e = \tfrac{1}{2}\bar{\phi}^{eT} \bar{\mathbf{K}}^e \bar{\phi}^e - \bar{\phi}^{eT} \mathbf{R}^e, \tag{35}$$

where $\bar{\phi}^e = \{\phi_u^e, \phi_w^e, \bar{\phi}_\theta^e\}$. The matrix $\bar{\mathbf{K}}^e$ is symmetrical. $\bar{\mathbf{K}}^e$ and $\mathbf{R}^e$ are the stiffness matrix and load vector for the beam.

The beam element is non-conforming other than at corners. As the number of terms in ϕ_n^e is increased, the incompatibility in normal rotation between the beam and the adjacent slab element tends to zero.

ASSEMBLY OF STIFFNESS EQUATIONS

The slab stiffness equations are combined with the stiffness equations of the adjoining beam elements to form a combined set of stiffness equations for the beam–slab macro element. These combined stiffness equations are assembled using standard finite element procedures. Only slight modifications are required to account for the variable degrees of freedom.

EXAMPLES

Two examples governed by full composite action were analysed to demonstrate the proposed technique. For simplicity, the same number of terms, denoted by M, is taken in all the series approximations.

Beam supported slab

The beam–slab structure shown in Fig. 7(a) was analysed using the idealized cross-section shown in Fig. 7(c). The loading consisted of a uniformly distributed load of 4 kPa. Young's modulus was taken as 20×10^3 MPa and Poisson's ratio was taken as 0.15. Beam properties were calculated using normal beam theory for flexure and axial loads using rectangular cross-sections of 450 mm × 150 mm. The torsional stiffness was based on St. Venant's theory of the same rectangular cross-section, with torsional stiffening effects of joining the beams to the slab being neglected. Hence the beam properties were $I = 1.139 \times 10^9\,\text{mm}^4$, $A = 67.5 \times 10^3\,\text{mm}^2$ and $J = 399.4 \times 10^6\,\text{mm}^4$.

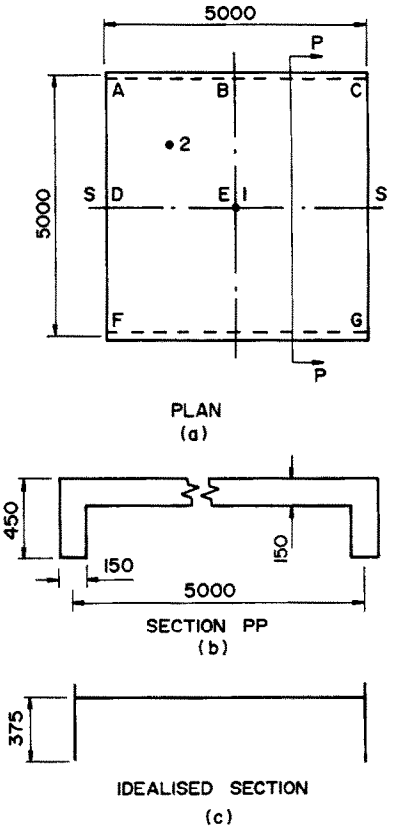

Fig. 7. Beam supported slab (all dimensions in millimetres). S = simple support.

Two analyses were performed using the macro elements. Firstly, the complete section ACGF was considered as a single element, which is the obvious discretization. Secondly, taking symmetry into account, the quarter section ABED was treated as a single element. Transverse displacements and plate bending moments at points 1 and 2 are given in Table 1 for varying values of M. The results are compared with a series solution [2] and a finite element solution. For the finite element solution, a quarter of the structure was discretized using a 12 × 12 uniform mesh. The slab elements combined the ACM plate bending element and a bilinear plane stress element [12]. A standard beam element was used.

As can be seen in Table 1, convergence is rapid for both displacement and moments. The results for the full section analysis are more accurate as in this case

Table 1. Results for beam supported slab

M	w_1 (mm)	w_2 (mm)	M_{x1} (kNm/m)	M_{x2} (kNm/m)
	Complete section analysis			
1	2.408	1.473	5.557	3.737
2	2.405	1.472	5.555	3.732
3	2.409	1.473	5.562	3.729
5	2.409	1.473	5.561	3.731
10	2.409	1.473	5.561	3.731
	Quarter section analysis			
1	2.428	1.475	5.582	3.733
2	2.408	1.473	5.618	3.733
3	2.409	1.473	5.561	3.732
4	2.409	1.473	5.583	3.732
5	2.409	1.473	5.565	3.731
10	2.409	1.473	5.565	3.731
FEM	2.412	1.475	5.573	3.742
Series	2.409	1.473	5.561	3.731

both points 1 and 2 are internal points of the macro element. This is consistent with previous observations [15, 16] which indicate that convergence for interior points is more rapid than for points on the boundary.

Composite floor system

Secondly, the composite steel–concrete floor system shown in Fig. 8 was analysed. This type of floor system has been discussed by Ansourian [5]. A comparison with Ansourian's results is not possible as the elastic properties used for the steel and concrete were not stated in Ansourian's work. Hence, the example was analysed using a finite element mesh as stated below. The loading consisted of a uniformly distributed load of 5 kPa. The idealizations made were similar to the previous example. For the slab, Young's modulus was taken as 2×10^4 MPa and Poisson's ratio was taken as 0.15, while for the beams Young's modulus was taken as 2×10^5 MPa and Poisson's ratio was taken as 0.3. Due to symmetry, there is no torsion in the supporting beams. The beam properties were $I = 85.2 \times 10^6$ mm^4, $A = 5150$ mm^2 and the beam–slab eccentricity was 226.9 mm. Taking symmetry into account, a quarter panel was analysed using a single macro element. The results are compared with a finite element solution using a uniform 12×12 mesh.

Transverse displacement, plate bending moments and beam bending moment (denoted by M_b) at various locations are given in Table 2. As can be seen in the table, convergence is rapid with few series terms. There is also good agreement with the finite element solution.

CONCLUSIONS

A macro element technique has been presented for the analysis of composite beam–slab systems. The technique combines a macro element to model the transverse bending and in-plane effects of the slab with a special beam element which couples the bending and in-plane effects. As complete solutions are used for the slab macro element, large elements corresponding to structural units may be used, resulting in minimum data preparation. As the com-

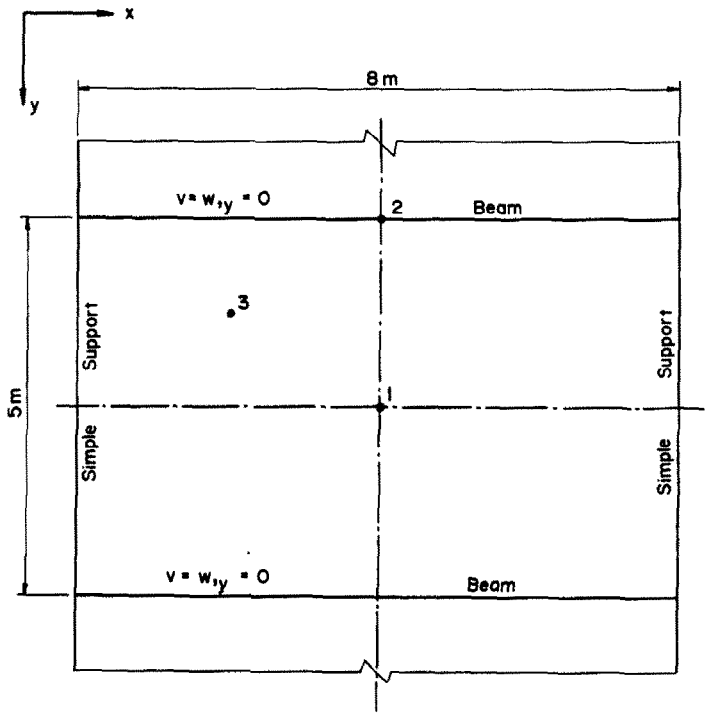

Fig. 8. Composite floor system.

Table 2. Results for composite floor system

M	w_1 (mm)	w_3 (mm)	M_{x1} (kNm/m)	M_{x2} (kNm/m)	M_{x3} (kNm/m)	M_{b2} (kNm)
1	15.09	10.48	13.44	11.29	9.725	36.48
2	15.05	10.49	13.40	11.28	9.765	36.56
3	15.06	10.49	13.16	11.22	9.753	36.37
4	15.06	10.49	13.21	11.20	9.753	36.33
5	15.06	10.49	13.16	11.18	9.751	36.29
10	15.06	10.49	13.15	11.16	9.752	36.23
FEM	15.09	10.51	13.19	11.28	9.795	36.57

bined beam–slab element has variable degrees of freedom, convergence is readily assessed. Engineering accuracy is obtained with the generation and solution of very few equations.

REFERENCES

1. R. H. Wood, *Studies in Composite Construction. Part 2: The Interaction of Floors and Beams in Multi-Storey Buildings*. HMSO, London (1955).
2. D. N. de G. Allen and R. T. Severn, Composite action of beams and slabs under transverse loadings. *Struct. Engng*. Part 1: **39,** 149–154 (1961); Part 2: **39,** 235–239 (1961); Part 3: **40,** 191–195 (1962); Part 4: **42,** 429–432 (1964).
3. K. Kretsis, Eccentric edge beams on bridge slabs. *Struct. Engng* **48,** 315–317 (1970).
4. M. A. Khan and K. O. Kemp, Elastic full composite action in a slab and beam system. *Struct. Engng* **48,** 353–359 (1970).
5. P. Ansourian, An application of the method of finite elements to the analysis of composite floor systems. *Proc. Inst. civ. Engrs* **59,** 699–726 (1975).
6. Y. K. Cheung, *Finite Strip Method in Structural Analysis*. Pergamon Press, Oxford (1976).
7. J. D. Davies, I. J. Somervaille and O. C. Zienkiewicz, Analysis of various types of bridges by the finite element method. In *Developments in Bridge Design and Construction* (Edited by K. C. Rockey, J. L. Bannister and H. R. Evans), pp. 217–236. Crosby Lockwood, London (1971).
8. M. M. Hrabok, Stiffened plate analysis by the hybrid stress finite element method. Ph.D. thesis, University of Edmonton, Canada (1981).
9. M. M. Hrabok and T. M. Hrudley, Finite element analysis in design of floor systems. *J. Struct. Div., ASCE* **109,** 909–925 (1983).
10. B. W. Golley and J. Petrolito, Method for analysing tanks and continuous plates. *Comput. Struct.* **18,** 1141–1151 (1984).
11. A. R. Cusens and R. P. Pama, *Bridge Deck Analysis*. John Wiley, New York (1975).
12. O. C. Zienkiewicz, *The Finite Element Method*, 3rd Edn. McGraw–Hill, New York (1977).
13. D. J. Fraser, The equivalent frame method simplified for beam and slab construction. *Concr. Int. Des. Constr.* **4,** 66–73 (1982).
14. D. J. Fraser, Elastic analysis of laterally loaded frames. *J. Struct. Div., ASCE* **109,** 1479–1489 (1983).
15. J. Petrolito and B. W. Golley, Plate bending analysis using macro elements. *Comput. Struct.* **28,** 407–419 (1988).
16. J. Petrolito and B. W. Golley, Plane stress analysis using macro elements. *Comput. Struct.* **31,** 553–565 (1989).
17. S. P. Timoshenko and S. Woinowsky-Krieger, *Theory of Plates and Shells*. McGraw–Hill, New York (1959).
18. S. P. Timoshenko and J. N. Goodier, *Theory of Elasticity*, 3rd Edn. McGraw–Hill, New York (1970).